X-Ray Absorption Spectroscopy (XAS): Surface Structural Determination of Alloy Nanoparticles

30

Guanghui Zhang, Nicole LiBretto, Stephen Purdy, Laryssa Cesar, and Jeffrey Miller

Contents

Abstract

In catalysis since reactions occur on the surface of nanoparticles (NP), it is essential to determine the composition of this structure, rather than that of the nanoparticles, since the two may be, and often are, different. Conventional techniques including X-ray absorption spectroscopy (XAS) and X-ray diffraction (XRD) are powerful techniques, but these data reflect the average composition of the entire particle. In this chapter, we introduce the method of EXAFS analysis, which isolates the surface atoms of nanoparticles based on its sensitivity to chemical reactions, specifically surface oxidation. As shown in our case studies, if the surface of a Pt-based nanoparticle is contacted by air at room temperature, the surface will selectively oxidize, resulting in the loss of Pt-Pt and Pt-M bonds to the formation of Pt-O bonds. The difference between the completely reduced and surface-oxidized nanoparticle allows for the isolation of signal from the catalytic surface. Although these examples highlight Pt alloys, similar analysis is also possible for other group 8 and IB bimetallic catalysts.

Keywords

Surface structure · Surface-sensitive X-ray absorption · Intermetallic alloy · Resonant inelastic X-ray scattering · Propane dehydrogenation · Pt alloy catalysts

G. Zhang
Davidson School of Chemical Engineering, Purdue University, West Lafayette, IN, USA

State Key Laboratory of Fine Chemicals, PSU-DUT Joint Center for Energy Research, School of Chemical Engineering, Dalian University of Technology, Dalian, Liaoning, People's Republic of China
e-mail: gzhang@dlut.edu.cn

N. LiBretto
Davidson School of Chemical Engineering, Purdue University, West Lafayette, IN, USA

Manufacturing Product Technology, Research & Development, Honeywell UOP, McCook, IL, USA
e-mail: Nicole.libretto@honeywell.com; nlibrett@purdue.edu

S. Purdy
Davidson School of Chemical Engineering, Purdue University, West Lafayette, IN, USA

Manufacturing Science Division, Oak Ridge National Laboratory, Oak Ridge, TN, USA
e-mail: purdysc@ornl.gov

L. Cesar
Davidson School of Chemical Engineering, Purdue University, West Lafayette, IN, USA

Dow Performance Silicones, Dow Chemical Company, Midland, MI, USA
e-mail: lcesar@dow.com

J. Miller (✉)
Davidson School of Chemical Engineering, Purdue University, West Lafayette, IN, USA
e-mail: mill1194@purdue.edu; jeffrey-t-miller@purdue.edu

I. E. Wachs, M. A. Bañares (eds.), *Springer Handbook of Advanced Catalyst Characterization*, Springer Handbooks,
https://doi.org/10.1007/978-3-031-07125-6_30

30.1 Introduction

The identification of the geometric and electronic structures of heterogeneous catalysts and their evolution under realistic reaction conditions is essential for developing structure-function relations that motivates catalyst development. With the availability of a new generation of synchrotron radiation facilities, scientists are now able to characterize catalytic nanomaterials under working conditions with control of specific reaction conditions (e.g., temperature, pressure, reactor configuration, and chemical feedstock). In particular, X-ray absorption spectroscopy (XAS) has been extensively used by the catalysis community to identify the oxidation state and geometric arrangement of atoms. This has further been enabled through the development of fast scan modes, allowing for the capture of information about key reaction intermediates and mechanistic steps in the catalytic cycle [1–5]. Many elements of interest in catalytic materials have absorption edges in the hard X-ray regime. This allows for a variety of in situ and *in operando* sample environments since hard X-rays can penetrate cell windows, gas or liquid reactants, support materials, etc. Hence, one can make measurements under realistic reaction conditions and detect all atoms of interest in the sample. While XAS measures every atom, which is important for understanding the nanoparticle structure, chemical reactions occur at the surface of heterogeneous catalysts, where the structure of the active sites may differ from the average composition [6–14]. A precise understanding of the surface structure in alloy nanoparticles, therefore, is critical for relating the active site structure to catalytic performance.

There are many excellent books and reviews on the theory and practice of XAS [15–24], and in this chapter, we will not introduce the basic principles but, instead, present a method for determination of the surface composition and structure in alloy nanoparticle and show its potential with three examples. In the first, the average nanoparticle composition of two Pt-Cr alloy catalysts is similar, but their catalytic performance is not, and this difference is related to the surface composition. The second is an example of PtCo alloys in which the surface structure is the same but the structure of the nanoparticle interior changes with varying metal loading. The third example describes the formation of bimetallic Pt-V catalysts with differing composition and average structure. While the catalytic surface structure and reaction performance are identical, to assess the changes in the energy of the valence orbitals responsible for catalysis, for example, by resonant inelastic X-ray scattering (RIXS), requires that the surface and bulk nanostructures are identical since the latter method is not surface-sensitive.

30.2 Surface XAS of Alloy Metal Nanoparticle Catalysts: Basic Approach

In monometallic Pt nanoparticle catalysts, CO or H_2 chemisorption is often used to determine the number of surface atoms, i.e., the dispersion. Alternatively, the catalytic surface can be selectively oxidized by O_2 at room temperature, and the dispersion can be determined by re-reduction of the oxidized surface by H_2 titration. For many (reduced) nanoparticle catalysts, especially for noble metals, ambient oxidation leads to selective oxidation of the (monolayer) catalytic surface. The surface EXAFS method takes advantage of this selective oxidation. In the fully reduced nanoparticle, all atoms are reduced, while, in the oxidized nanoparticle, the surface atoms are oxidized, but the interior atoms remain reduced. For surface EXAFS analysis, the spectra of both the reduced and oxidized catalyst are determined. Subtraction of the oxidized from the reduced EXAFS gives a difference spectrum that allows for determination of the surface structure. See references [6, 9, 10, 25], and for more details on the procedure for this analysis. Since the interior atoms in both the reduced and oxidized nanoparticle are unchanged, these interior atoms subtract and are not present in the difference spectrum leaving only EXAFS from surface atoms. Specifically, there are fewer metallic atoms in the oxidized sample, while oxidation also leads to new M-O bonds. The difference spectrum (reduced – oxidized) has metal-metal scattering with phases identical to those in the reduced catalyst, while the M-O bonds are π-radians out of phase (due to the subtraction process) from a normal scattering pair [6, 9, 10, 25]. As will be demonstrated in the examples, this method works well when the fraction of surface atoms is large enough to get a reliable EXAFS in the difference spectrum, for example, nanoparticle less than about 5 nm in size where there are greater than about 20% surface atoms. For nanoparticle larger than about 8 nm, the error in the difference EXAFS fit becomes larger due to the small CNs, although qualitative characterization is still possible. The potential of the surface EXAFS technique will be demonstrated in the following three examples.

30.3 Case Study 1: Incomplete Formation of a Pt_3Cr Surface Alloy

Pt-Cr bimetallic catalysts show promising performance for propane dehydrogenation with propylene selectivity higher than 95% compared to monometallic Pt nanoparticles [10]. $2\%Pt/SiO_2$ (denoted 2Pt), $2\%Pt\text{-}1\%Cr/SiO_2$ (denoted 2Pt-1Cr), and $2\%Pt\text{-}3\%Cr/SiO_2$ (denoted 2Pt-3Cr) were

prepared by incipient wetness impregnation, and all catalysts had a similar particle size of about 2 nm measured by scanning transmission electron microscopy (STEM). Detailed structural characterization and catalytic performance have been previously reported [10]. Therefore, only a brief summary will be given here to demonstrate why it is necessary to determine the surface structure and how this can be determined using the surface EXAFS analysis. The propane dehydrogenation selectivity of 2Pt shows lower propylene selectivity (75%) than 2Pt-1Cr (95%) and 2Pt-3Cr (98%) at ~15% conversion. Additionally, the selectivity of 2Pt and 2Pt-1Cr decreases with increasing propane conversion, while that of 2Pt-3Cr remains little changed at all conversions, Fig. 30.1.

The crystalline phases (long-range order) and coordination environment (local structure) of 2Pt and 2Pt-3Cr were determined using in situ X-ray diffraction (XRD) and XAS, respectively. The XRD pattern of 2Pt-3Cr after reduction at 800 °C showed that the bimetallic phase was a Pt_3Cr intermetallic alloy. Under these conditions, the XAS indicated that a Pt has about 8 Pt neighbors and 4 Cr neighbors, with a Pt-Cr to Pt-Pt coordination number ratio ($CN_{Pt\text{-}Cr:Pt\text{-}Pt}$) of 0.5, consistent with the Pt_3Cr phase (Cu_3Au structure type). However, when 2Pt-3Cr was reduced at 550 °C under the conditions of the catalytic reaction, XRD indicates that both Pt and Pt_3Cr phases were present. The XAS was also consistent with a Pt-rich morphology with the $CN_{Pt\text{-}Cr:Pt\text{-}Pt}$ ratio of about 0.25. For 2Pt-1Cr reduced at 550 °C, the XRD pattern and EXAFS $CN_{Pt\text{-}Cr:Pt\text{-}Pt}$ ratio and bond distances were nearly identical to that of 2Pt-3Cr indicating that both catalysts have very similar average structures (Fig. 30.2). The catalytic performances, however, suggest some difference in the surface compositions.

As discussed above, the XAS difference spectrum of the reduced minus oxidized catalyst, depicted in Fig. 30.3, provides surface-sensitive structural information for the two Pt-Cr catalysts. Figure 30.4a shows the two Fourier transform of the k^2-weighted EXAFS spectra (reduced and oxidized) for 2Pt-3Cr. Upon room temperature oxidation, there is a small loss of surface Pt-Pt and Pt-Cr bonds and the formation of Pt-O bonds. Cr-O bonds formed from the oxidation of surface chromium in the alloy are not observed at the Pt edge due to the element specificity of XAS. While the oxidized spectrum could be fit directly to determine the core composition, the small changes and overlapping features make quantification of these changes in coordination numbers and bond distances less accurate for determination of the surface composition. By subtracting the oxidized from reduced EXAFS spectrum, Fig. 30.4b, changes in the two catalysts are more readily resolved and can be more accurately fit, Table 30.1.

The Pt-Cr to Pt-Pt coordination numbers, bond distances, and $CN_{Pt\text{-}Cr:Pt\text{-}Pt}$ ratio can be used to determine the Cr incorporation into these nanoparticles for the fully reduced alloy, metallic core (in the oxidized nanoparticle), and surface monolayer (from the difference EXAFS), Table 30.2. In the average EXAFS fit of 2Pt-3Cr, i.e., the reduced catalyst, the coordination ratio, $CN_{Pt\text{-}Cr:Pt\text{-}Pt}$, was 0.30, while that of the surface EXAFS is near 0.5. The latter is consistent with a stoichiometric Pt_3Cr intermetallic alloy

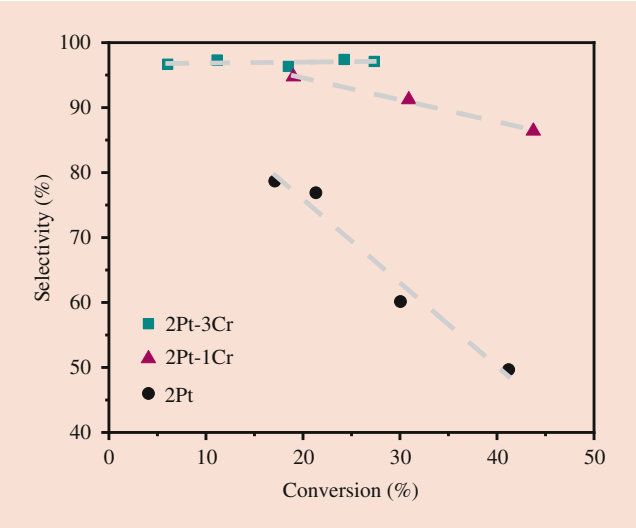

Fig. 30.1 Propylene selectivity as a function of propane dehydrogenation conversion at 550 °C, 2.5% C_3H_8 and 2.5% H_2 (balanced with N_2)

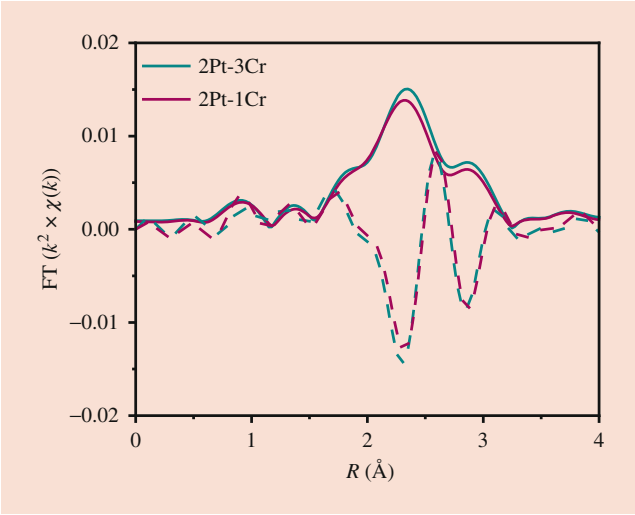

Fig. 30.2 EXAFS of Pt-Cr bimetallic nanoparticles containing 1 wt% and 3 wt% Cr after reduction at 550 °C in 3.5% H_2

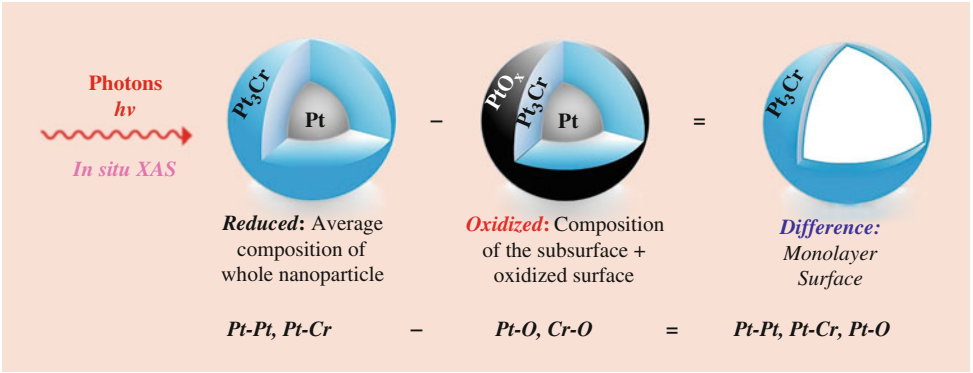

Fig. 30.3 Approach for difference analysis, where reduced Pt-Cr nanoparticles are subsequently oxidized and the EXAFS (chi) data is subtracted to isolate the surface atoms [10]

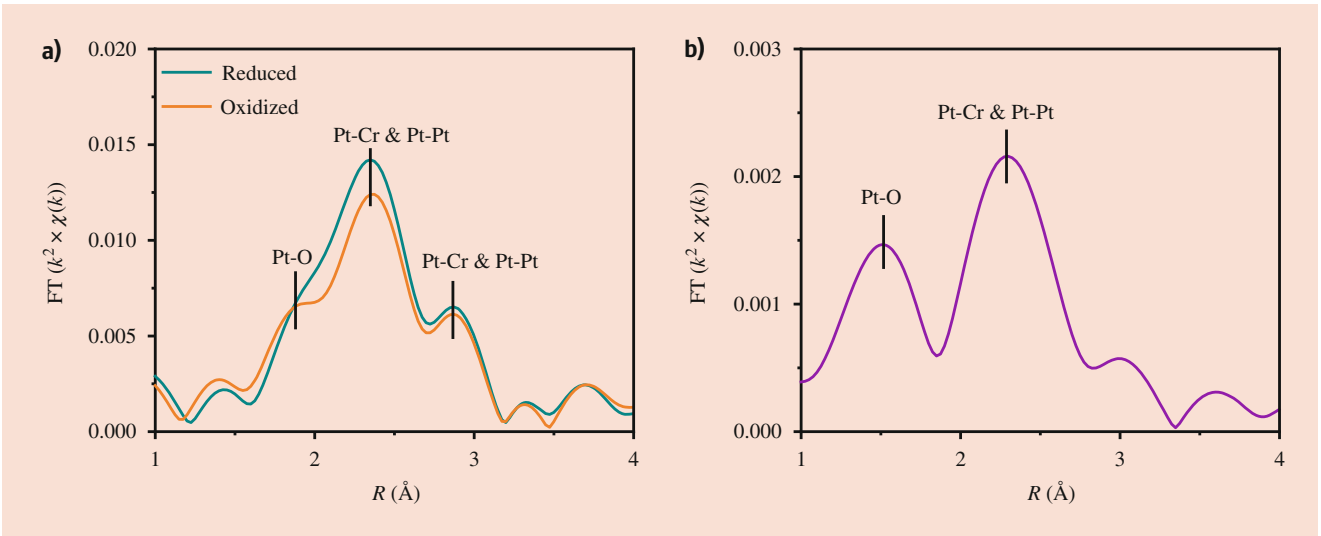

Fig. 30.4 The k^2-weighted Fourier transform of chi of 2Pt-3Cr after reduction at 550 °C; (**a**) the reduced, oxidized, and (**b**) difference EXAFS

Table 30.1 Difference EXAFS fits for 2Pt-1Cr and 2Pt-3Cr

Catalyst	Scattering pair	CN	*R* (Å)
2Pt-1Cr	Pt-Pt	1.5	2.75
	Pt-Cr	0.6	2.71
	Pt-O	0.4	2.05
2Pt-3Cr	Pt-Pt	0.9	2.73
	Pt-Cr	0.5	2.73
	Pt-O	0.3	2.05

Table 30.2 The $CN_{Pt\text{-}Cr}/CN_{Pt\text{-}Pt}$ ratios of 2Pt-1Cr and 2Pt-3Cr catalysts

Sample	$CN_{Pt\text{-}Cr}/CN_{Pt\text{-}Pt}$ ratio			Catalyst structure
	Average	Interior	Surface	
2Pt-1Cr	0.28	0.25	0.40	
2Pt-3Cr	0.30	0.22	0.56	

surface. The bond distances of the surface EXAFS are also consistent with the Pt_3Cr intermetallic alloy. The oxidized EXAS fit also represents the structure of the non-surface atoms in the nanoparticle, i.e., the nanoparticle core. Although the surface is a Pt_3Cr phase, the interior is much more Pt-rich than the surface. The analysis of the surface and particle interior also suggests that Cr alloy formation during synthesis starts at the surface of a reduced Pt nanoparticle with metallic Cr atoms diffusing to the nanoparticle interior.

A similar difference surface EXAFS analysis of the reduced and oxidized 2Pt-1Cr shows that the surface $CN_{Pt\text{-}Cr:Pt\text{-}Pt}$ ratio is 0.40 compared to 0.56 for the 2Pt-3Cr catalyst. In other words, the surface of 2Pt-1Cr is Pt-rich suggesting incomplete formation of a surface Pt_3Cr monolayer (Table 30.2), which leads to lower catalytic selectivity. By identifying the surface structures and compositions, small changes in the catalytic performance can be explained. For

these two catalysts, the 2Pt-3Cr had a full monolayer Pt_3Cr intermetallic alloy composition, while the surface of the 2Pt-1Cr was an incomplete monolayer; see schematic in Table 30.2. For the 2Pt-1Cr catalyst, even reduction at higher temperatures did not lead to a complete surface alloy monolayer [10].

30.4 Case Study 2: Identification of the Evolution of the Core-Shell Structures

In this example, using the difference surface EXAFS analysis, we show that the average Pt-Co NP composition changes with increasing Co loading, while the surface composition remains similar [9]. The average EXAFS of bimetallic Pt-Co nanoparticles containing 2 wt% Pt with 0.6 (2Pt-0.6Co), 1 (2Pt-1Co), 2 (2Pt-2Co), and 4 wt% Co (2Pt-4Co) is compared to a monometallic Pt nanoparticle (3Pt). The k^2-weighted magnitude of the Fourier transform (FT) at the Pt L_3 edge shows different shapes between the four bimetallic particles and Pt (Fig. 30.5 and Table 30.3). The shape of the EXAFS spectrum of 2Pt-0.6Co particles is distorted compared to monometallic Pt. The EXAFS fitting results suggest 7.8 Pt-Pt bonds at 2.73 Å and 2.5 Pt-Co bonds at 2.56 Å. The larger Pt-Pt coordination number is consistent with Pt-rich nanoparticles. As the nominal Co content increases, the number of Pt-Pt bonds decreases, and the number of Pt-Co bonds increases. For instance, 2Pt-1Co has 4.5 Pt-Pt bonds at 2.73 Å and 2.2 Pt-Co bonds at 2.56 Å (Table 30.3). The Pt-Co to Pt-Pt coordination number ratio ($CN_{Pt\text{-}Co:Pt\text{-}Pt}$) is about 0.5, which matches the Pt_3Co phase. This structure was also confirmed by in situ synchrotron XRD. In 2Pt-2Co, the number of Pt-Pt bonds decreases to 3.0, and the number of Pt-Co bonds increases to 2.9, i.e., a $CN_{Pt\text{-}Co:Pt\text{-}Pt}$ of about 1.0, or about an equal number of Pt-Pt and Pt-Co bonds. With a further increase in Co, in 2Pt-4Co, the $CN_{Pt\text{-}Co:Pt\text{-}Pt}$ ratio was approximately 2.0. Thus, with increasing Co loading, the average nanoparticle composition changes from Pt-rich to Co-rich from low to high loading, respectively.

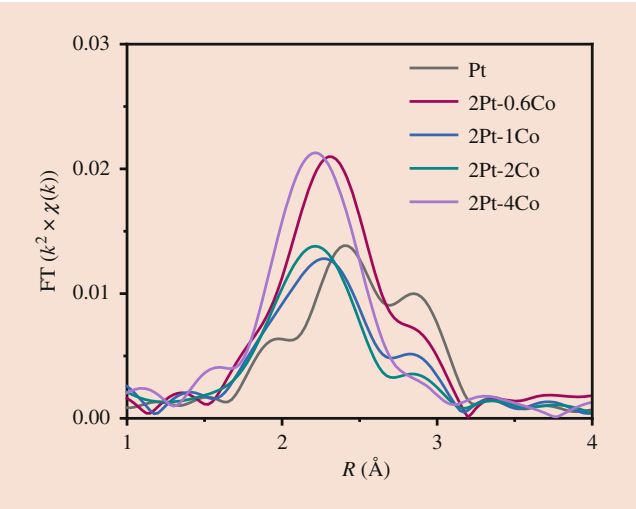

Fig. 30.5 Comparison of EXAFS magnitudes of Pt and Pt-Co catalysts

Since these nanoparticles are small (1–2 nm), there is a sufficiently large fraction of surface atoms, and the difference EXAFS analysis can be performed to identify the surface composition. Upon oxidation, there are loss of surface Pt-Pt and Pt-Co metallic bonds. The remaining metallic bonds in the spectra (Pt-Co and Pt-Pt), therefore, are due to metallic atoms from the nanoparticle interior, i.e., the nanoparticle core. From the difference EXAFS, it is possible to evaluate whether the composition is homogeneous throughout the particle or if the surface and particle interior have different compositions. In addition, the ratio of Pt-Co to Pt-Pt neighbors can be useful to identify the ordered surface structure or, at least, rule out other compositions and structures.

The reduced, oxidized, and difference spectra of 2Pt-1Co are shown in Fig. 30.6. In Fig. 30.6a, the large peaks (solid line between about 2–3 Å) of the reduced catalysts represent both Pt-Pt and Pt-Co bonds. The red spectrum in Fig. 30.6a shows the oxidized spectrum with loss of metallic neighbors and addition of a Pt-O peak at about 1.5 Å (phase uncorrected distance). In these bimetallic Pt-Co catalysts, since the fraction of surface atoms is high, there is a significant Pt-O peak, which can be fit. In the difference spectrum, any atoms that are unchanged are not present in the difference spectrum.

Table 30.3 Summary of EXAFS analysis for the reduced bimetallic and monometallic Pt and Co samples

Sample	Scattering pair	Bond length (Å)	CN	$CN_{Pt\text{-}Co:Pt\text{-}Pt}$	Phase
3Pt	Pt-Pt	2.75	9.3	0	Pt
2Pt-0.6Co	Pt-Pt	2.73	7.8	0.32	Pt + Pt_3Co
	Pt-Co	2.56	2.5		
2Pt-1Co	Pt-Pt	2.73	4.5	0.49	Pt_3Co
	Pt-Co	2.56	2.2		
2Pt-2Co	Pt-Pt	2.73	3.0	0.97	Pt_3Co + PtCo
	Pt-Co	2.56	2.9		
2Pt-4Co	Pt-Pt	2.73	2.5	2.08	Pt_3Co + PtCo
	Pt-Co	2.56	5.2		

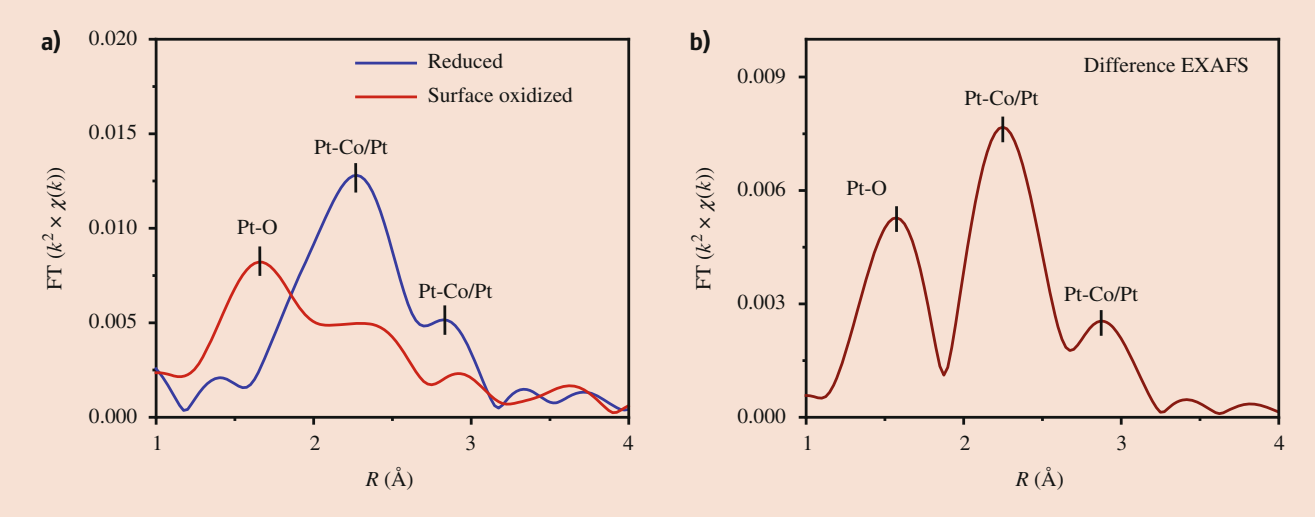

Fig. 30.6 FT magnitude of the EXAFS for 2Pt-1Co at the Pt L_3 edge

Table 30.4 Fitting results for the difference spectra (reduced minus oxidized catalyst) at the Pt L_3 edge

Sample	Bond	Bond length (Å)	CN	$CN_{Pt\text{-}Co:Pt\text{-}Pt}$
3Pt	Pt-O	2.05	0.9	–
	Pt-Pt	2.77	2.5	–
2Pt-0.6Co	Pt-O	2.05	0.2	–
	Pt-Pt	2.73	0.6	0.5
	Pt-Co	2.56	0.3	
2Pt-1Co	Pt-O	2.05	0.9	–
	Pt-Pt	2.73	2.1	0.5
	Pt-Co	2.56	1.0	
2Pt-2Co	Pt-O	2.05	0.9	–
	Pt-Pt	2.73	2.4	0.5
	Pt-Co	2.56	1.2	
2Pt-4Co	Pt-O	2.05	0.7	–
	Pt-Pt	2.73	1.9	0.5
	Pt-Co	2.56	0.9	

Thus, the Pt-Pt, Pt-Co, and Pt-O are more easily resolved and fit in the difference EXAFS spectrum (Fig. 30.6b). The fits for the difference EXAFS are shown in Table 30.4.

An unexpected result in Table 30.4 is that the $CN_{Pt\text{-}Co:Pt\text{-}Pt}$ is near 0.5 for all catalysts, despite the clear difference in their average and core compositions. This suggests that all catalysts likely have the same surface structure, i.e., Pt_3Co (structure type $AuCu_3$) with different core compositions from Pt-rich to Pt_3Co to PtCo.

As also shown in Fig. 30.6, the difference EXAFS gives a Pt-O scattering peak, which can be related to the number of surface Pt atoms in the alloy. For alloy nanoparticles, the STEM particle size gives the fraction of surface atoms, but not the number of catalytic surface atoms. In addition, as in the case of Pt-Co alloys, since both Pt and Co may adsorb standard adsorbates like H_2 and CO, the Pt and Co dispersions are not possible to determine. However, the Pt dispersion can be estimated from the Pt-O coordination number. For example, Pt(II) compounds have CNs of 4, thus the Pt dispersion is the ratio of Pt-O CN/4 in the difference spectrum. The accuracy of the Pt-O coordination number is more accurate in the difference EXAFS than in the partially oxidized sample, since there is less overlap of the Pt-O and metallic Pt scatters; see Figs. 30.4b and 30.6b, for example. This energy specificity of the surface Pt-O allows for determination of the number of catalytic sites for determination of the turnover rates and identification of the active site, for example, Pt or Co [9].

30.5 Case Study 3: Identification of Bimetallic Alloy Compositions Suitable for Determination of Electronic Changes by XANES or RIXS Spectroscopy

While the surface alloy composition and structure are important, there are also important electronic changes in the energy of the catalytic, i.e., surface, valence orbitals, which control the metal-reactant bond energies, surface coverage, and performance. For the row 5 catalytic elements, e.g., Pt, the L_2 and L_3 edge XANES measure the energy of the unfilled 5d orbitals, while resonant inelastic X-ray scattering (RIXS) allows for determination of the energy of the filled 5d orbitals. Both XANES and RIXS measure all atoms in the sample and, thus, are not surface-sensitive. The absorption and emission processes for RIXS are shown in Fig. 30.7 [26–30]. It is the energy of the filled 5d orbitals of the surface-active atoms that is responsible for the catalytic performance. As shown in the case studies above, the composition of bimetallic catalysts is often not uniform, and the surface can have a different composition from that of the average nanoparticle. Since hard X-rays sample all atoms in

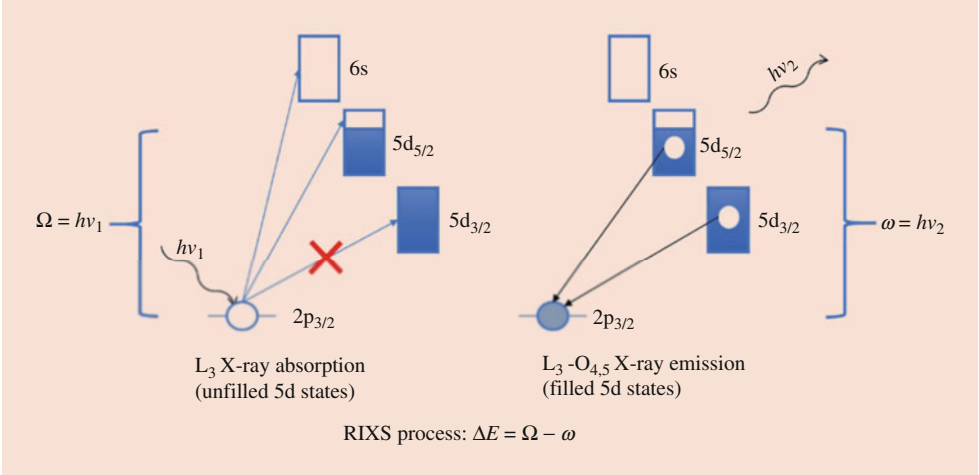

Fig. 30.7 RIXS spectroscopy: excitation of the 2p electron to the empty 5d orbitals (XANES absorption spectra) and decay to the core hole from the filled 5d state (emission spectrum). The difference in energy of the absorbed (Ω) and emitted (ω) photon gives the energy difference between filled and unfilled 5d valence orbitals

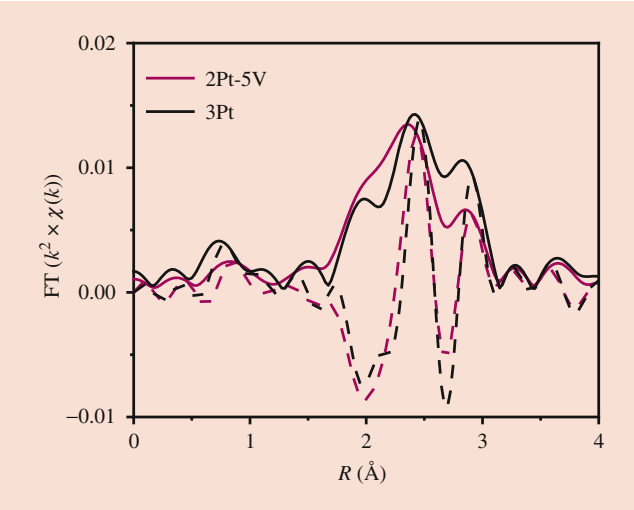

Fig. 30.8 R-space EXAFS magnitude (solid lines) and imaginary components (dashed lines) for 2Pt-5V/SiO_2 and 3Pt/SiO_2 collected after reduction in hydrogen at 550 °C

the catalyst, in order to accurately determine the energy shifts due to catalytic surface, one must measure the XANES, and RIXS, on catalysts where the nanoparticle and surface compositions are identical, i.e., a fully alloyed nanoparticle with the same surface and interior structure. The following example shows two Pt-V bimetallic alkane dehydrogenation catalysts with similar catalytic selectivity and rates but differ in their structure. Determination of the nanoparticle and surface structures allows for identification of the catalyst in which all atoms have identical geometry and electronic properties allowing for accurate determination of the changes in energy of the Pt valence orbitals due to alloy formation with V [25].

A 3%Pt/SiO_2 catalyst (denoted 3Pt) and two Pt-V/SiO_2 catalysts with different Pt loadings, 2%Pt-5%V/SiO_2 (2Pt-5V) and 5%Pt-5% V/SiO_2 (5Pt-5V), were synthesized, and full characterization of the structures and catalytic performance have been previously reported [25]. Thus, only a brief summary is given. All three catalysts had metal particle sizes of approximately 2.5 nm. Both Pt-V catalysts had propylene selectivity above 95% at 20% propane conversion and comparable propylene turnover rates of 0.3 ± 0.1 s^{-1}. The bimetallic structure of the catalyst was verified using in situ EXAS, Fig. 30.8. The 3Pt catalyst showed scattering from Pt neighbors, with three characteristic peaks between 2 and 3 Å. The ratio of the three peaks in the 2Pt-5V catalyst is modified due to Pt-V scattering. First shell fits of the two spectra are given in Table 30.5. The coordination number ratio of Pt-V to Pt-Pt ($CN_{Pt\text{-}V:Pt\text{-}Pt}$) for 5Pt-5V was 0.31, while the ratio for 2Pt-5V was 0.47, demonstrating that 5Pt-5V was Pt-rich compared to 2Pt-5V. The coordination number ratio of Pt_3V intermetallic alloy is 0.5, suggesting that the 2Pt-5V nanoparticles are a full alloy, while those in 5Pt-5V are a phase mixture, i.e., Pt + Pt_3V.

Table 30.5 XANES energies and EXAFS fitting results for 3Pt and two Pt-V catalysts reduced at 550 °C

Sample	Edge energy (keV)	Scattering pair	CN	*R* (Å)
3Pt	11.5640	Pt-Pt	8.8	2.74
5Pt-5V	11.5642	Pt-Pt	6.5	2.73
		Pt-V	2.0	2.71
2Pt-5V	11.5644	Pt-Pt	6.2	2.72
		Pt-V	2.9	2.72

The nanoparticle surface compositions of 2Pt-5V and 5Pt-5V were determined using the difference EXAFS spectra (reduced – oxidized) and are shown in Fig. 30.9, and fits are given in Table 30.6. Both spectra show Pt-O scattering between 1 and 2 Å from the surface oxidation process and Pt-Pt and Pt-V scattering between 2 and 3 Å. Fitting the difference spectra and taking the ratio of $CN_{Pt\text{-}V}$ to $CN_{Pt\text{-}Pt}$ gave a ratio close to 0.5 for both catalysts, which is consistent with their similar catalytic performance and suggests a Pt_3V surface structure. While the surface and bulk ratio for 2Pt-5V were similar, suggesting a pure-phase Pt_3V nanoparticle, the

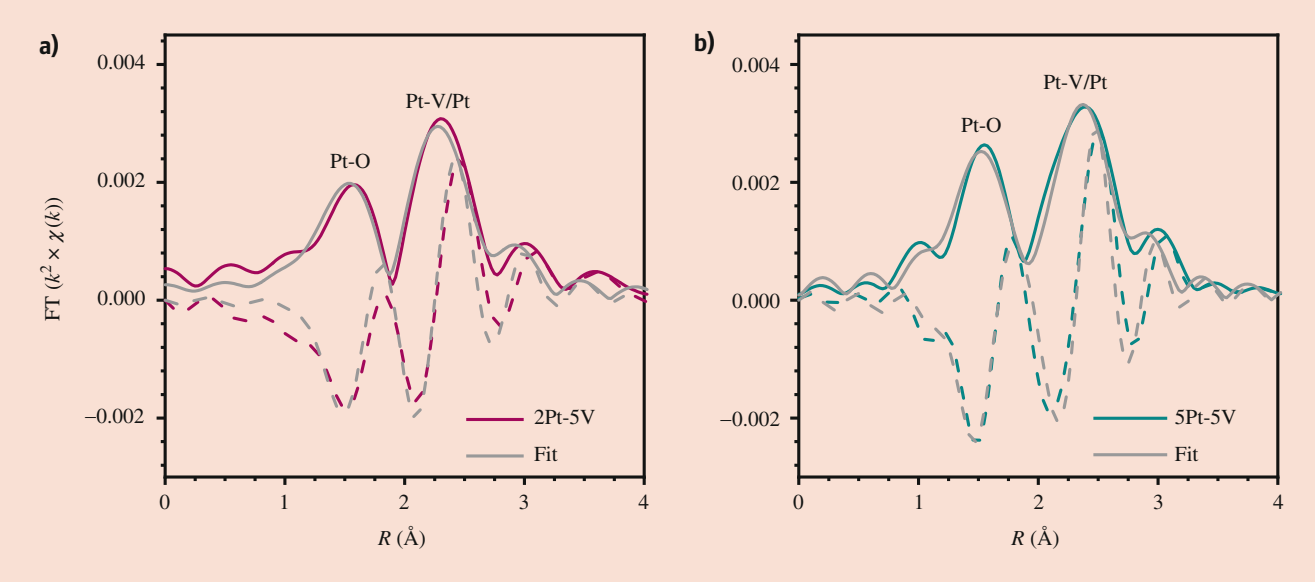

Fig. 30.9 Pt EXAFS difference spectra for 2Pt-5V (**a**) and 5Pt-5V (**b**) and difference spectra fit

Table 30.6 EXAFS fit for Pt-V difference spectra

Sample	Scattering pair	CN	*R* (Å)	CN_{Pt-V}/CN_{Pt-Pt} ratio
5Pt-5V	Pt-O	0.6	2.03	0.58
	Pt-Pt	1.2	2.74	
	Pt-V	0.7	2.74	
2Pt-5V	Pt-O	0.5	2.05	0.66
	Pt-Pt	0.9	2.70	
	Pt-V	0.6	2.72	

bulk coordination ratio of 5Pt-5V was lower than that of the surface suggesting a structure with a Pt-rich core and a Pt_3V shell consistent with the in situ synchrotron XRD.

Consistent with changes in average coordination geometry in the bimetallic Pt-V catalyst, the XANES spectra and edge energies shift slightly to higher energy with increasing V content in the nanoparticles suggesting changes in the energy of the unfilled Pt 5d orbitals; see Fig. 30.10 and Table 30.5. For the 5Pt-5V and 2Pt-5V bimetallic catalysts, there is a shift to higher energy, 11.5642 and 11.5644 keV, respectively, compared to Pt (11.5640 keV); however, edge energy of 5Pt-5V is the average of atoms in the NP, Pt_3V + Pt, rather than the catalytic surface, i.e., Pt_3V. Only in the 2Pt-5V is the surface composition and structure the same as the NP. Thus, the true shift in the energy of the empty Pt 5d orbitals between Pt and Pt_3V phases is an increase of 0.4 eV. Thus, to obtain accurate determination of the electronic properties of the catalytic surface, i.e., the Pt_3V phase, one not only has to determine the nanoparticle composition but also confirm that the surface and bulk structures are the same.

Since the average and surface EXAFS of 2Pt-5V indicate a full Pt_3V intermetallic alloy, the RIXS spectrum was obtained and compared to that of Pt, Fig. 30.11. The energy transfer is the difference in energy between the absorbed (XANES) and emitted photons. When the energy transfer is combined with the XANES energy, the energy of the filled 5d orbitals, which are responsible for adsorbate bonding and surface chemistry, can be determined. For Pt, the energy transfer value is 2.7 eV. For Pt_3V, the energy transfer value is larger, 3.5 eV. The energy separation between the filled and unfilled states in Pt_3V is 0.8 eV larger than Pt, which can be separated into a 0.4 eV increase in the energy of the unfilled states and a 0.4 eV decrease in the energy of the filled 5d states relative to Pt. These values in Pt 5d orbital energies reflect the true nature of the electronic changes due to the Pt_3V alloy and, thus, are comparable with density functional theory (DFT) calculations and essential for understanding of the catalytic properties [25].

30.6 Summary

Bimetallic nanoparticles often have complex morphologies where the average and surface structures differ significantly. In the examples highlighted in this chapter, a method is presented which allows for determination of the surface structure even though hard X-rays sample all atoms in the nanoparticle. The difference EXAFS approach relies on the selective oxidation of surface atoms. While these examples were for Pt alloys, the method is not limited to noble metals. For example, the surface atoms of Cu(0) nanoparticles can be selectively oxidized to Cu(I) forming a surface Cu_2O layer. The quantity of Cu(I) sites generated during N_2O oxidation could be used to estimate the number of active Cu(0) surface sites [31]. Since in the Cu_2O surface layer each Cu(I) site is surrounded by two oxygen atoms, the increase of the Cu-O coordination number could also be used to determine the

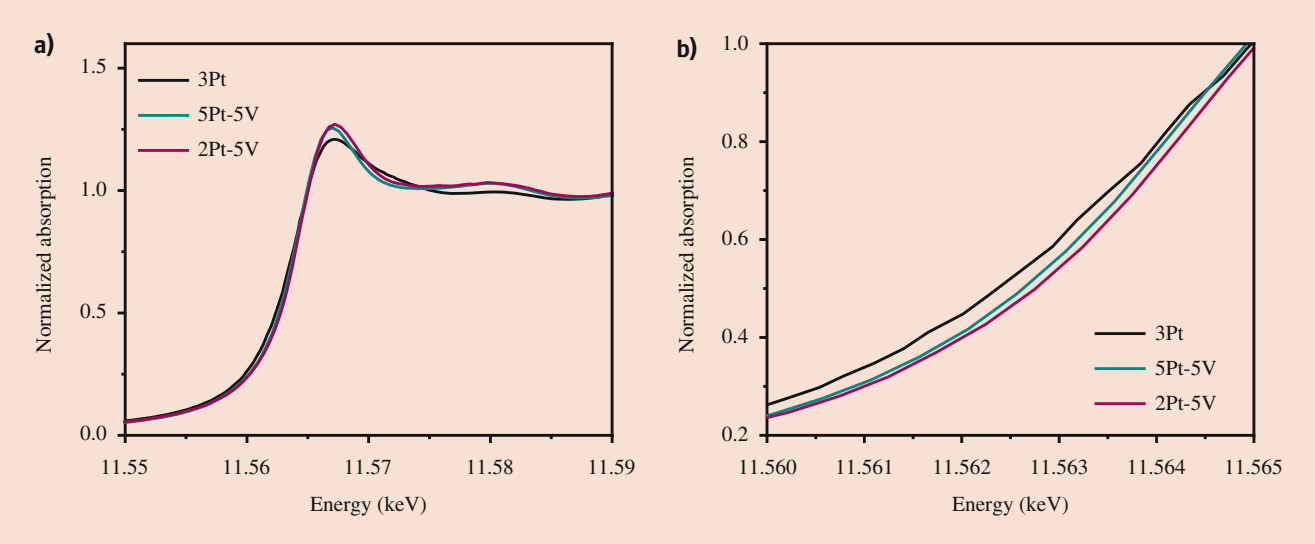

Fig. 30.10 (**a**) In situ Pt L_3 edge XANES of 3Pt/SiO_2, 2Pt-5V/SiO_2, and 5Pt-5V/SiO_2; (**b**) zoomed-in region of the XANES spectra. Spectra were collected at room temperature in He after reduction at 550 °C in 3.5% H_2

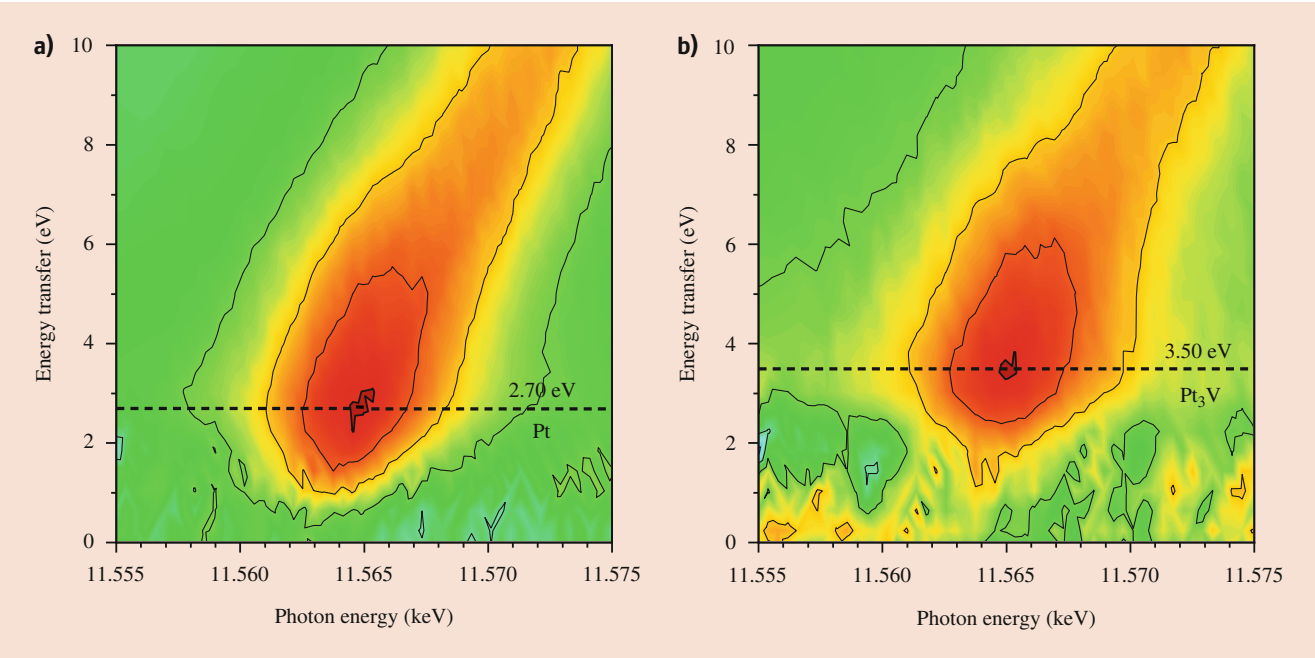

Fig. 30.11 (**a**) Pt L_3-Lβ_5 RIXS maps of 3Pt and (**b**) 2Pt-5V (Pt_3V). Spectra were collected after a reduction treatment at 550 °C in 3.5% H_2. Horizontal dashed lines denote the maximum of energy transfer (difference in the absorbed and emitted photons) for each catalyst

surface composition of Cu catalysts. For particle sizes of less than about 5 nm, there is a sufficient fraction of surface atoms to provide accurate surface analysis. For example, in the study of the bimetallic Pt-V catalysts [25], there are small differences in XRD patterns of Pt and Pt_3V, which makes identification of the intermetallic alloy structure or solid solutions difficult, especially for small nanoparticles where the peaks are small and broad and can overlap. The surface EXAFS coordination ratio can also be useful for elimination of several possible alloy structures, for example, that are inconsistent with the fits. In addition, comparison of the NP and surface EXAFS can also rule out the formation of solid solutions. For the latter, the surface and average composition are the same, while for intermetallic alloys core-shell structure are common, i.e., regions of different composition [25]. Finally after elimination of these structures, the NP (for

2Pt-5V) and surface CN ratios (and XRD) were consistent with formation of the Pt_3V intermetallic alloy.

While these examples focused on differences in surface and average structures resulting from different compositions, this method is equally applicable to changes in the surface composition under reaction including changes due to the reacting gases, deactivation, or poisoning. The basis of this technique relies on changes in the surface structure during a chemical reaction. Here the reaction was surface oxidation but could also be applied to changes in the catalyst under reaction conditions. For example, deactivation may lead to M-C surface bonds, sintering, or surface reconstruction. For coke formation one would expect to determine new M-C scatting peaks, which could be fit to determine the CN, i.e., $C/M_{surface}$ and M-C bond distance. Sintering would lead to increases in the average NP CN, while the surface CN would decrease. Finally, surface reconstruction would lead to changes in surface composition, and the difference EXAFS before and after reaction would show which Ms have lower and higher surface concentrations after reaction. The full potential of the method is to determine these changes in the surface during reaction, deactivation, etc.

Acknowledgments

This chapter is based on work supported by the National Science Foundation under cooperative agreement no. EEC-1647722. GZ would like to acknowledge the National Natural Science Foundation of China (21902019) and Fundamental Research Funds for the Central Universities (DUT18RC(3)057 and DUT20RC(5)002). Use of the Advanced Photon Source was supported by the US Department of Energy, Office of Basic Energy Sciences, under contract no. DE-AC02-06CH11357. MRCAT operations, beamline 10-BM, are supported by the Department of Energy and the MRCAT member institutions. The authors also acknowledge the use of beamline 11-ID-C at APS.

References

1. Zhang, G., Yi, H., Zhang, G., Deng, Y., Bai, R., Zhang, H., Miller, J.T., Kropf, A.J., Bunel, E.E., Lei, A.: Direct observation of reduction of Cu(II) to Cu(I) by terminal alkynes. J. Am. Chem. Soc. **136**, 924–926 (2014)
2. Macmillan, S.N., Lancaster, K.M.: X-ray spectroscopic interrogation of transition-metal-mediated homogeneous catalysis: primer and case studies. ACS Catal. **7**, 1776–1791 (2017)
3. Paolucci, C., Khurana, I., Parekh, A.A., Li, S., Shih, A.J., Li, H., Di Iorio, J.R., Albarracin-Caballero, J.D., Yezerets, A., Miller, J.T., Delgass, W.N., Ribeiro, F.H., Schneider, W.F., Gounder, R.: Dynamic multinuclear sites formed by mobilized copper ions in NOx selective catalytic reduction. Science. **357**, 898–903 (2017)
4. Zhang, G., Yi, H., Xin, J., Deng, Y., Bai, R., Huang, Z., Miller, J.T., Kropf, A.J., Bunel, E.E., Qi, X., Lan, Y., Lei, A.: Aromatic C–H bond cleavage by using a Cu(i) ate-complex. Org. Chem. Front. **3**, 975–978 (2016)
5. Wan, G., Zhang, G., Lin, X.-M.: Toward efficient carbon and water cycles: emerging opportunities with single-site catalysts made of 3d transition metals. Adv. Mater. **32**, 1905548 (2020)
6. Wu, Z., Bukowski, B.C., Li, Z., Milligan, C., Zhou, L., Ma, T., Wu, Y., Ren, Y., Ribeiro, F.H., Delgass, W.N., Greeley, J., Zhang, G., Miller, J.T.: Changes in catalytic and adsorptive properties of 2 nm Pt3Mn nanoparticles by subsurface atoms. J. Am. Chem. Soc. **140**, 14870–14877 (2018)
7. Ye, C., Wu, Z., Liu, W., Ren, Y., Zhang, G., Miller, J.T.: Structure determination of a surface tetragonal Pt1Sb1 phase on Pt nanoparticles. Chem. Mater. **30**, 4503–4507 (2018)
8. Zhang, G., Ye, C., Liu, W., Zhang, X., Su, D., Yang, X., Chen, J.Z., Wu, Z., Miller, J.T.: Diffusion-limited formation of nonequilibrium intermetallic nanophase for selective dehydrogenation. Nano Lett. **19**, 4380–4383 (2019)
9. Cesar, L.G., Yang, C., Lu, Z., Ren, Y., Zhang, G., Miller, J.T.: Identification of a Pt3Co surface intermetallic alloy in Pt–Co propane dehydrogenation catalysts. ACS Catal. **9**, 5231–5244 (2019)
10. LiBretto, N.J., Yang, C., Ren, Y., Zhang, G., Miller, J.T.: Identification of surface structures in Pt3Cr intermetallic nanocatalysts. Chem. Mater. **31**, 1597–1609 (2019)
11. Zhu Chen, J., Wu, Z., Zhang, X., Choi, S., Xiao, Y., Varma, A., Liu, W., Zhang, G., Miller, J.T.: Identification of the structure of the bi promoted Pt non-oxidative coupling of methane catalyst: a nanoscale Pt3Bi intermetallic alloy. Cat. Sci. Technol. **9**, 1349–1356 (2019)
12. Wu, Z., Wegener, E.C., Tseng, H.-T., Gallagher, J.R., Harris, J.W., Diaz, R.E., Ren, Y., Ribeiro, F.H., Miller, J.T.: Pd–In intermetallic alloy nanoparticles: highly selective ethane dehydrogenation catalysts. Cat. Sci. Technol. **6**, 6965–6976 (2016)
13. Wegener, E.C., Wu, Z., Tseng, H.-T., Gallagher, J.R., Ren, Y., Diaz, R.E., Ribeiro, F.H., Miller, J.T.: Structure and reactivity of Pt–in intermetallic alloy nanoparticles: highly selective catalysts for ethane dehydrogenation. Catal. Today. **299**, 146–153 (2018)
14. Shen, X., Zhang, C., Zhang, S., Dai, S., Zhang, G., Ge, M., Pan, Y., Sharkey, S.M., Graham, G.W., Hunt, A., Waluyo, I., Miller, J.T., Pan, X., Peng, Z.: Deconvolution of octahedral Pt3Ni nanoparticle growth pathway from in situ characterizations. Nat. Commun. **9**, 4485 (2018)
15. Frenkel, A.I.: Applications of extended X-ray absorption fine-structure spectroscopy to studies of bimetallic nanoparticle catalysts. Chem. Soc. Rev. **41**, 8163–8178 (2012)
16. Newville, M.: Fundamentals of XAFS. *Rev. Mineral. Geochem.* **78**, 33–74 (2014)
17. Silvia, B., Elena, G., Giovanni, A., Van Bokhoven, J.A., Carlo, L.: Reactivity of surface species in heterogeneous catalysts probed by in situ X-ray absorption techniques. *Chem. Rev.* **113**, 1736–1850 (2013)
18. Koningsberger, D.C., Prins, R.: X-Ray Absorption Principles, Applications, Techniques of EXAFS, SEXAFS and XANES. Wiley (1988)
19. Bunker, G.: Introduction to XAFS. Cambridge University Press (2010)
20. Calvin, S.: XAFS for Everyone. CRC Press (2013)
21. Rehr, J.J., Albers, R.C.: Theoretical approaches to X-ray absorption fine structure. Rev. Mod. Phys. **72**, 621–654 (2000)
22. Bokhoven, J.A.V., Lamberti, C.: X-Ray Absorption and X-Ray Emission Spectroscopy: Theory and Applications. Wiley (2016)
23. Nelson, R.C., Miller, J.T.: An introduction to X-ray absorption spectroscopy and its in situ application to organometallic compounds and homogeneous catalysts. Cat. Sci. Technol. **2**, 461–470 (2012)
24. Frenkel, A.I., Rodriguez, J.A., Chen, J.G.: Synchrotron techniques for in situ catalytic studies: capabilities, challenges, and opportunities. ACS Catal. **2**, 2269–2280 (2012)
25. Purdy, S.C., Ghanekar, P., Mitchell, G., Kropf, A.J., Zemlyanov, D.Y., Ren, Y., Ribeiro, F., Delgass, W.N., Greeley, J., Miller, J.T.: The origin of electronic modification of platinum in a Pt3V alloy and

their consequences for propane dehydrogenation catalysis. ACS Appl. Energy Mater. **3**, 1410–1422 (2020)
26. Ravel, B., Kropf, A.J., Yang, D., Wang, M., Topsakal, M., Lu, D., Stennett, M.C., Hyatt, N.C.: Nonresonant valence-to-core X-ray emission spectroscopy of niobium. Phys. Rev. B. **97** (2018). https://doi.org/10.1103/PhysRevB.97.125139
27. Cybulskis, V.J., Bukowski, B.C., Tseng, H.-T., Gallagher, J.R., Wu, Z., Wegener, E., Kropf, A.J., Ravel, B., Ribeiro, F.H., Greeley, J., Miller, J.T.: Zinc promotion of platinum for catalytic light alkane dehydrogenation: insights into geometric and electronic effects. ACS Catal. **7**, 4173–4181 (2017)
28. Glatzel, P., Sikora, M., Smolentsev, G., Fernández-García, M.: Hard X-ray photon-in photon-out spectroscopy. Catal. Today. **145**, 294–299 (2009)
29. Pieter, G., Jagdeep, S., Kvashnina, K.O., Van Bokhoven, J.A.: In situ characterization of the 5d density of states of Pt nanoparticles upon adsorption of CO. *J. Am. Chem. Soc.* **132**, 2555–2557 (2010)
30. Wegener, E.C., Bukowski, B.C., Yang, D., Wu, Z., Kropf, A.J., Delgass, W.N., Greeley, J., Zhang, G., Miller, J.T.: Intermetallic compounds as an alternative to single-atom alloy catalysts: geometric and electronic structures from advanced X-ray spectroscopies and computational studies. ChemCatChem. **12**, 1325–1333 (2020)
31. Hanukovich, S., Dang, A., Christopher, P.: Influence of metal oxide support acid sites on cu-catalyzed nonoxidative dehydrogenation of ethanol to acetaldehyde. ACS Catal. **9**, 3537–3550 (2019)

Guanghui Zhang received his PhD at Wuhan University in 2014. He spent several years as a postdoc researcher at Illinois Institute of Technology and Purdue University. He joined Dalian University of Technology in 2018. His current research interests include energy and environment-related catalysis and synchrotron-based in situ X-ray techniques.

Nicole LiBretto is a PhD candidate at the Davidson School of Chemical Engineering at Purdue University. She graduated with a Bachelor of Engineering from Stony Brook University in 2016. Her research is with Dr. Jeffrey T. Miller in developing new catalyst compositions for shale gas conversion.

Stephen Purdy received his PhD in chemical engineering from Purdue University in 2019, where he studied platinum and palladium intermetallic compounds for light alkane dehydrogenation by synchrotron X-ray techniques. He is currently a postdoc in the diffraction group at the spallation neutron source, Oak Ridge National Laboratory studying catalyst structure by X-ray and neutron total scattering.

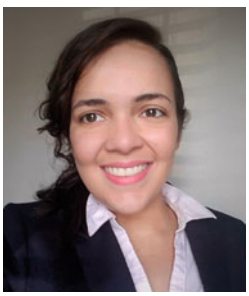

Laryssa Cesar received her PhD at Purdue University in 2019. She joined Dow Chemical Company shortly after in 2019. She currently works as a Senior Research Specialist in the Dow Performance Silicones Business. Her current research interests include silicone-related heterogeneous and homogeneous catalysis as well as development and scale up of new processes.

Jeffrey Miller spent 25 years working in industry R&D for Amoco-BP. In 2008 he became the heterogeneous catalysis group leader at Argonne National Laboratory and has been a professor in chemical engineering at Purdue University since 2015. His research interests include energy and environment-related catalysis, especially the characterization of catalysts using in situ synchrotron-based X-ray characterizations.